Eur. Phys. J. B **8**, 67–72 (1999)

THE EUROPEAN PHYSICAL JOURNAL B

EDP Sciences

Magnetic field induced instabilities of a doped lyotropic hexagonal phase

L. Ramos[1,a], P. Fabre[2], and L. Fruchter[3]

[1] Laboratoire de Physique de la Matière Condensée[b], Collège de France, 11 place Marcelin Berthelot, 75231 Paris Cedex 05, France
[2] UMR CNRS-Elf Atochem, 95 rue Danton, 92303 Levallois-Perret Cedex, France
[3] Laboratoire de Physique des Solides, Bâtiment 510, Université Paris-Sud Orsay, 91405 Orsay Cedex, France

Received 10 February 1998

Abstract. A new anisotropic magnetic fluid is obtained using a colloidal suspension of magnetic particles of nanometric size (ferrofluid) as a component of a swollen lyotropic hexagonal phase. This doped hexagonal system exhibits specific behaviors when submitted to a magnetic field of weak intensity. The field-induced instabilities are described and interpreted; they result from a high anisotropy of the magnetic susceptibility of the medium, which is measured. It is finally shown that the magnetic properties of the doped hexagonal phase allows one a determination of the compression modulus of the system.

PACS. 75.50.Mm Magnetic liquids – 82.70.Dd Colloids – 61.30.Gd Orientational order of liquid crystals; electric and magnetic field effects on order

1 Introduction

Recently we have realized a hybrid colloidal assembly of a new type [1], which combines a lyotropic hexagonal matrix with a suspension of colloidal magnetic particles (ferrofluid). The magnetically doped system thus obtained consists of a triangular array of liquid apolar cylinders into which solid magnetic particles of nanometric size are incorporated (Fig. 1). One of the distinctive features of this system is that the combination of a high magnetic susceptibility ferrofluid and a uniaxial hexagonal phase results in a unidimensional magnetic liquid. The bidimensional equivalent system, the ferrosmectic phase, which consists of ferrofluid layers separated by the surfactant membranes of a lamellar phase [2], has been extensively studied. In regard of the results concerning its magnetic properties [3,4], one can expect that magnetically doped hexagonal phases should also give a specific response to an external magnetic field.

In this paper, we explore the magnetic properties of magnetically doped hexagonal samples. After a brief recall of the sample characteristics, we first describe and interpret the magnetic instabilities that the doped system develops when submitted to a magnetic field of weak intensity. We next present a study of the anisotropy of magnetic susceptibility of the hexagonal phase. The experimental results investigated as a function of the particle concentration are quantitatively interpreted. In the last part, we present a determination of one elastic constant of the hexagonal phase directly derived from the magnetic experiments and then discuss the results.

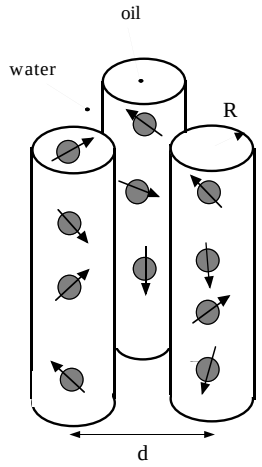

Fig. 1. Sketch of the magnetically doped hexagonal phase.

2 Samples

The samples are prepared in the hexagonal phase region of the phase-diagram of a pseudo-quaternary mixture

[a] *Present address*: Groupe de Dynamique des Phases Condensées, Cc 26, Université Montpellier 2, place E. Bataillon, 34095 Montpellier Cedex 5, France.
e-mail: `ramos@gdpc.univ-montp2.fr`
[b] CNRS, URA 792

(sodium dodecyl sulfate, pentanol, cyclohexane and brine, [NaCl] = 0.4 M). The structure of the swollen hexagonal phases is fully described elsewhere [5] and consists of oil cylinders of radius 150 Å, including the surfactant tails, which are immersed in the aqueous medium and arranged in a triangular array with a lattice parameter $d =$ 325 Å. The magnetically doped samples are obtained by incorporating solid ferrimagnetic iron oxide (maghemite, γ-Fe_2O_3) particles [6,7] inside the lyotropic cylinders, up to a particle volume fraction Φ (relative to cyclohexane) of 2%. A complete characterization of the doped system by X-ray scattering has shown the existence of a depletion layer for the particles near the inner walls of the cylinders, the particles are thus quasi-unidimensionally confined in the center of the tubes [1]. Moreover, the existence of this depletion layer seems to prevent any direct mechanical coupling between the nanoparticles and the lyotropic matrix.

Let us briefly describe the characteristics of the suspension of magnetic particles (ferrofluid). The particles, dispersed in cyclohexane, are stabilized against Van der Waals attractions by a surfactant coating; their size distribution is log-normal with mean radius $r_0 = 35$ Å – the radius refers here to the solid core – and a standard deviation $\sigma = 0.35$, as determined by small-angle X-ray scattering (SAXS). The geometric radius of the particles, including the surfactant layer, is about 51 Å. The particles are small enough to be magnetic monodomains and thus bear a permanent moment $m_0 = M_s v$, where v is the volume of the particle and M_s is the maghemite bulk magnetization ($M_s = 3.75 \times 10^5$ A m^{-1}). In zero magnetic field, the colloidal suspension exhibits no magnetization because of Brownian motion. When an external field is applied, the particles moments align parallel to the field, leading to a magnetization M that obeys the Langevin law for paramagnetism: the ferrofluid is said to be superparamagnetic [8]. The superparamagnetic susceptibility χ_0 is given by the initial slope of the $M(H)$ curve [9]:

$$\chi_0 = \frac{4\pi\mu_0 M_s^2}{9kT} r_0^3 \exp(13.5\,\sigma^2)\Phi_0 = \alpha_0 \Phi_0. \qquad (1)$$

The susceptibility is proportional to the volume fraction in particles, Φ_0. From the X-ray scattering determination of the size distribution of the particles, one gets: $\alpha_0 = 13.4$. This value might be slightly over-evaluated since the X-ray experiments give a measure of the iron core of the particle, including the non-magnetic shell at the surface.

3 Effect of a magnetic field

3.1 Experiments

The samples are held in glass capillaries of rectangular section 1×0.1 mm^2 and the cylinders are oriented along the long axis of the capillary (z) with the following process: the hexagonal phase is first cooled down to an isotropic state ($\sim 8\,°$C) and then slowly heated up to room temperature under a homogeneous and constant magnetic field ($H \sim 10$ kOe), along which the cylinders align. However the perfectly oriented sample is very fragile, and most of the time the sample exhibits a striated texture commonly encountered with lyotropic hexagonal phases [5,10–12], which corresponds to collective undulations of the columns around their mean direction, in (y, z) planes parallel to the main sides of the capillary.

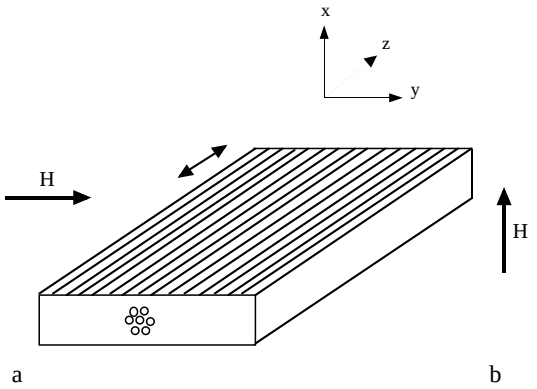

Fig. 2. (a) "planar" and (b) "normal" configurations for the study of the reorientation under a magnetic field. The double arrow indicates the initial direction of the cylinders.

Two different geometric configurations are explored with respect to the orientation of the magnetic field (Fig. 2): in both cases, a field is applied perpendicularly to the axis of the cylinders but it is either normal (along x), "normal geometry", or parallel (along y), "planar geometry", to the anchoring walls of the cell. The magnetic fields of fixed intensity, as measured with a Hall effect probe, are produced by small permanent magnets, in the gap of which the capillary is positioned. The samples are observed by polarized light microscopy, the analyzer and polarizer lying in the (y, z) plane. The kinetics is very slow for fields of weak intensity: the time scales to consider are between a few hours and a few weeks, for the range of intensities explored (up to about 1 kOe). In the following, we describe the effects occurring in the two geometric configurations.

3.1.1 Normal geometry

Above a threshold field, one observes a reorientation of the cylinders along the magnetic field. Because of the very slow kinetics, the determination of a threshold field is delicate. We arbitrarily set the maximum duration for the observation to two weeks. With this convention, for samples with $\Phi = 0.5\%$, one gets for the threshold field: $300 < H_c^n < 400$ Oe. The large uncertainty is related to the experimental protocol defined above.

When a sample is submitted to a field higher than the critical one, the reorientation occurs through the appearance of a homogeneous striated texture (Fig. 3); the stripes are parallel to the initial z direction of the cylinders. It is important to underline that the nature of the stripes is different from the striated textures that can be initially present. Indeed, the field related striped texture disappears when either the polarizer or the analyzer is

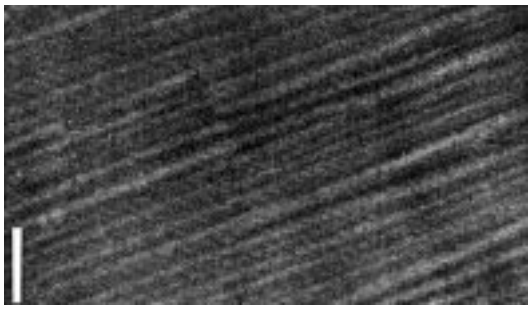

Fig. 3. Striation pattern developed in the normal geometry (magnetic field perpendicular to the plane of observation). Bar = 100 μm.

parallel to the initial direction (z) of the cylinders, which indicates that the distortion of the optical axis occurs in the plane defined by their initial direction (z) and the direction of the field (x). On the contrary, the striations which form spontaneously correspond to distortions in the plane (y, z). The periodicity of the pattern (of the order of 10 μm) increases with time, whilst it becomes less and less birefringent and regular. Finally the sample appears completely dark between crossed polarizers whatever their orientation, indicating a homeotropic orientation. The initial texture is recovered when the field is removed, which is the signature of a strong anchoring at the walls.

3.1.2 Planar geometry

The overall effect is, in this geometry also, a reorientation of the cylinders along the magnetic field above a threshold value, but the observed stages of the process of reorientation appear more complex than in the normal geometry. First, the determination of a threshold field is more delicate, because the nature of the field induced striations is equivalent to the possible spontaneous striations. One can nevertheless determine a magnetic field below that no evolution of this striated pattern is observed. For example, one finds $70 < H_c^p < 95$ Oe, for Φ equal to 0.5%. Let us remark that this field is about four times smaller than the threshold field determined in the case of the normal geometry.

For fields higher than H_c^p but lower than about 400 Oe, a striped texture is maintained during the whole sequence, whose periodicity increases with time, and this texture becomes less well-defined and regular, as cylinders reorient along the magnetic field. On the contrary, for higher fields ($>$ 400 Oe), the striped texture degenerates into a striking well-defined herring-bone pattern (Fig. 4), whose periodicity also increases with time. The herring-bone corresponds to periodically localized distortions of the optical axis within a stripe, such that in the distorted zone, the angle between the optical axis and the magnetic field is smaller. This texture recalls the twisted texture that occurs with cholesteric polymer liquid crystal [11,13] when the concentration in polymer increases so as to relax mechanical constraints. In our case, it is very likely that magnetic constraints are relaxed in that way.

Fig. 4. Herring-bone pattern developed in the planar geometry (the arrow indicates the direction of the magnetic field). Bar = 100 μm.

In both cases, the final state corresponds to cylinders parallel to the field. When the magnetic field is removed at early stages (*i.e.* when the deformations are small), the initial texture is recovered, whereas it is not at later stages.

3.2 Interpretation

The first important observation to stress is that, whatever the geometry (planar or normal), the transition from the initial state where the cylinders lie perpendicular to the magnetic field to the final state, with cylinders parallel to the field, is homogeneous. This is opposite to that observed with lamellar phases doped with magnetic particles. For these bidimensional systems, the application of a magnetic field perpendicular to the layers has indeed been found to induce a reorientation of these layers via a heterogeneous occurrence of toroidal defects [4]. On the contrary, in the present experiments, the homogeneous striated texture recalls the well-known Helfrich-Hurault instabilities for cholesteric and smectic phases [14,15], and experiments will be interpreted with this comparison in mind.

First of all, the rotation of the structure in the field suggests that doped hexagonal phases possess an anisotropic magnetic susceptibility. Indeed, the ferrofluid suspension is an isotropic superparamagnetic medium described by a scalar susceptibility χ_0, but once the suspension is incorporated inside a hexagonal lyotropic structure, because of the axial symmetry, the susceptibility is expected to be a tensor with two components:

$$\tilde{\chi} = \begin{pmatrix} \chi_\perp & 0 & 0 \\ 0 & \chi_\perp & 0 \\ 0 & 0 & \chi_\parallel \end{pmatrix}$$

where $\chi_\perp$ and $\chi_\parallel$ are respectively the magnetic susceptibilities in a plane orthogonal to the optical axis of the medium and parallel to the optical axis. The difference between the two components, $\chi_a = \chi_\parallel - \chi_\perp$, is called the anisotropy of magnetic susceptibility of the medium.

The density of magnetic energy of a hexagonal phase submitted to a magnetic field $\mathbf{H}$ can be written as $F_{magn.} = (1/2)\mu_0\chi_a \left|\mathbf{H}\wedge\mathbf{t}\right|^2$ where $\mathbf{t}$ is the direction of the axis of the cylinders. Experiments clearly indicate that χ_a is positive, so that an orientation of the cylinders parallel to the applied field is energetically more favorable than a perpendicular one.

In the following, we focus on the normal geometry: indeed, the strength of the anchoring in the planar configuration being more questionable, a quantitative interpretation of the threshold field would be delicate. In the normal geometry, one can use the analogy with the Helfrich-Hurault instabilities for smectic phases [16], which correspond to undulations of the optical axis in planes defined by the initial direction of the optical axis and the direction of the field above a threshold field. The threshold field results from a competition between the magnetic energy and the elastic deformation energy. For modes polarized in the (x,z) planes, smectic and hexagonal systems behave identically [16]. Thus, a straightforward extrapolation of the smectic results predicts the expression for the threshold field:

$$H_c^n = \left[\frac{2\pi\sqrt{K_3\left(\bar{B}+C\right)}}{\mu_0\chi_a h}\right]^{1/2} . \qquad (2)$$

The $\bar{B}$, C and K_3 constants are defined in the expression of the density of free energy F for an elastic deformation of a hexagonal phase [16,17]:

$$F = \frac{1}{2}\bar{B}\left(\nabla_\perp\cdot u\right)^2 + \frac{1}{2}C\Big[\left(\nabla_x\cdot u_y + \nabla_y\cdot u_x\right)^2 + \left(\nabla_x\cdot u_x - \nabla_y\cdot u_y\right)^2\Big] + \frac{1}{2}K_3\left(\nabla_\parallel^2 u\right)^2 \qquad (3)$$

K_3 is the column bending elasticity, $\bar{B}$ is the elastic constant corresponding to homogeneous compression of the triangular lattice of columns, C is a constant for a shear deformation of the lattice; $\bar{B}+C$ is an uniaxial compression modulus.

The expression (2) for the threshold field shows that quantitative information of the elasticity of the doped system could be gained from the threshold field measurement if the anisotropy of magnetic susceptibility is known. This has been one of the motivations for carrying out an experimental study of this parameter, which is presented in the next part.

4 Study of the anisotropic magnetic susceptibility

4.1 Experiments

The samples are held in small cylindrical cells of inner diameter 0.95 mm and length of the order of 5 mm. A SQUID magnetometer (Quantum Design Inc.) equipped with a superconducting magnet is used to measure the sample magnetization for discrete values of the field. Because of the reduced available space inside the magnetometer, the cell that contains the sample can only be positioned with its main axis (z) parallel to the field. This implies that, in order to measure the magnetization curve with both the field parallel and perpendicular to the cylinders, one has to produce two orientations of the cylinders with respect to the cell. The procedure we adopted is the following: prior to the magnetic measurement, we align the cylinders perpendicular to the z axis of the cell with a high magnetic field ($\sim 8\times10^4$ Oe); this geometry allows the measurement of the perpendicular magnetization $M_\perp$. From the initial slope of the $M_\perp(H)$ curve, one has thus access to the perpendicular susceptibility $\chi_\perp$. We then apply *in situ* a high magnetic field that reorients the cylinders parallel to the long axis of the cell; the field is applied sufficiently long to ensure a complete reorientation. This allows the measurement in a second step of the parallel magnetization $M_\parallel$. The initial slope of the $M_\parallel(H)$ curve gives thus access to the parallel susceptibility $\chi_\parallel$; this slope is always larger than initial slope for the $M_\perp(H)$ curve: the system exhibits thus a positive anisotropy of susceptibility $\chi_a = \chi_\parallel - \chi_\perp > 0$. We have checked that there is no relaxation towards the most favorable parallel orientation (for which the cylinders are parallel to the anchoring walls) on the time scale of the $\chi_\perp$ measurements (about 20 min).

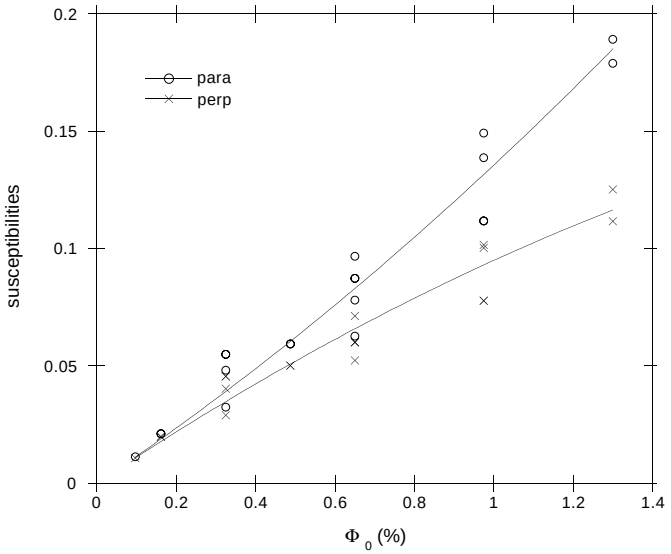

Fig. 5. Variation of the parallel and perpendicular susceptibilities with the volume fraction of particles. The lines correspond to fits with second order polynomials: $\chi_\parallel = 11.3\,\Phi_0 + 228\,\Phi_0^2$ and $\chi_\perp = 11.3\,\Phi_0 - 178\,\Phi_0^2$.

We vary the particle volume fraction Φ relative to cyclohexane from 0.15 to 2%, which corresponds to volume fraction Φ_0 relative to the whole volume in the range 0.10–1.34% and investigate the behavior of both the perpendicular and parallel susceptibilities with Φ_0. Notice that, because of the large aspect ratio of the cell, the effect of the demagnetizing field due to the shape anisotropy of the cell is here negligible [18] and the intrinsic susceptibilities are equal to the measured ones. The variations of both the parallel $\chi_\parallel$ and perpendicular $\chi_\perp$ are reported in Figure 5. The uncertainties arise essentially

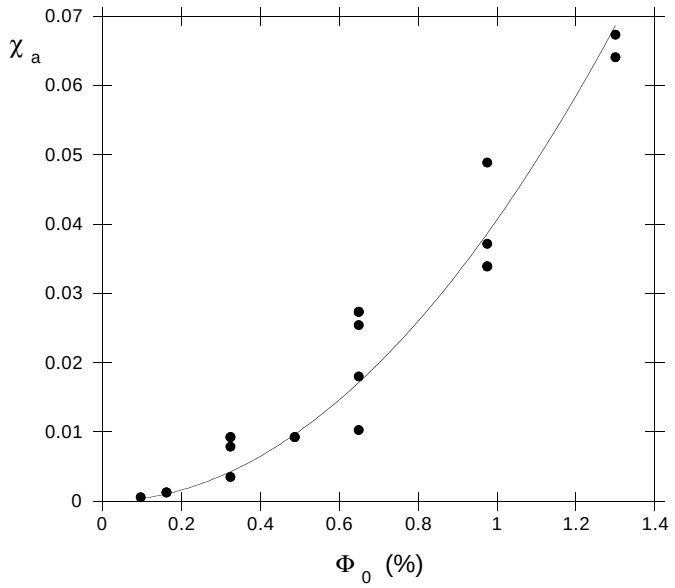

Fig. 6. Variation of the anisotropy of susceptibility with the volume fraction in particles. The line corresponds to a quadratic function: $\chi_a = 406\,\Phi_0^2$.

from the experimental determination of the volume of the samples. The anisotropy of magnetic, χ_a, are reported in Figure 6. The values are in the range 4×10^{-4}–7×10^{-2}. The data clearly shows a quadratic dependence of χ_a with Φ_0; the best fit gives: $\chi_a = 406\,\Phi_0^2$. Concerning the parallel and perpendicular susceptibilities, their variations appear essentially linear with Φ_0, indicating that the quadratic parts are small compared to the linear ones. Fits with second order polynomials give: $\chi_\parallel = 11.3\,\Phi_0 + 228\,\Phi_0^2$ and $\chi_\perp = 11.3\,\Phi_0 - 178\,\Phi_0^2$.

4.2 Interpretation

One can *a priori* analyze the anisotropy of magnetic susceptibility at different spatial scales. First, one can treat the system as a periodic arrangement of continuous paramagnetic tubes whose intrinsic susceptibility is χ_0, the susceptibility of the tridimensional ferrofluid, separated by a non-magnetic medium [19]. But, as the radius of the ferrofluidic cylinders is comparable to the size of the particles, so that each magnetic cylinder is quasi-unidimensional, this first approach is questionable. It seems thus more reasonable to use a mean-field type model and consider an assembly of magnetic particles distributed in lines: each particle is submitted to an external field, plus the dipolar field created by its neighbors, which is different whether the external field is parallel or perpendicular to the lines. The doped hexagonal phase is modeled as a bidimensional lattice of these lines. The number of particles per unit length is N_l, and each particle bears an effective moment $\mathbf{m}$ along the field. We note a, the total radius for the particles, that includes the surfactant length ($2a = 102$ Å corresponds to the distance at contact). In a first stage, we calculate the dipolar fields created at the center of a line by the magnetic moments of this line. Following Widom [20] and Ponsinet [3], the dipolar field $\mathbf{H}_d^i$, $i = (\parallel, \perp)$, is:

$$\mathbf{H}_d^\parallel = \int_{|r|>a} \frac{N_l \mathbf{m}}{4\pi r^3} \left[3 \left(\frac{\mathbf{m}}{m} \frac{\mathbf{r}}{r} \right) \frac{\mathbf{r}}{r} - \frac{\mathbf{m}}{m} \right] dr = \frac{N_l \mathbf{m}}{2\pi a^2} \tag{4}$$

when the external field is parallel to the cylinders, and

$$\mathbf{H}_d^\perp = \frac{N_l \mathbf{m}}{4\pi a^2} \tag{5}$$

when the external field is perpendicular to the cylinders.

With a calculation analogous to the calculation for Lorentz local fields in a polarizable medium [21], it is shown [22] that the dipolar fields, parallel and perpendicular, created in the center of a tube by the corona of neighboring tubes are equal to zero. Thus, the relations (4, 5) given above are available for the hexagonally packed arrangement of columns. The magnetization is

$$M = \frac{N_l m}{\pi R^2} \rho_c = \frac{2 N_l m}{\sqrt{3} d^2},$$

where ρ_c is the fraction of surface occupied by the cylinders of radius R in a plane orthogonal to their long axis. From $M_i = \chi_0 \left(H_{ext} + H_d^i \right) = \chi_i H_{ext}$, we then find to the second order in Φ_0:

$$\chi_\parallel = \frac{\chi_0}{1 - \frac{\chi_0 \sqrt{3} d^2}{4\pi a^2}} \approx \alpha_0 \Phi_0 \left(1 + \frac{\alpha_0 \Phi_0 \sqrt{3} d^2}{4\pi a^2} \right) \tag{6}$$

$$\chi_\perp = \frac{\chi_0}{1 + \frac{\chi_0 \sqrt{3} d^2}{8\pi a^2}} \approx \alpha_0 \Phi_0 \left(1 - \frac{\alpha_0 \Phi_0 \sqrt{3} d^2}{8\pi a^2} \right) \tag{7}$$

and

$$\chi_a \approx \frac{3\sqrt{3} d^2}{8\pi a^2} \alpha_0^2 \Phi_0^2. \tag{8}$$

In these expressions, the quadratic dependence of χ_a on Φ_0 is consistent with experimental results. Coming to a more quantitative comparison with the experimental data, the model predicts that the ratio $(\chi_\parallel - \alpha_0 \Phi_0)/(\alpha_0 \Phi_0 - \chi_\perp)$ is equal to 2, compared to the value of 1.3 extracted from the fits. On the other hand, from the fit of the parallel and perpendicular susceptibilities, one gets $\alpha_0 = 11.6$, compared to 13.4 for a theoretical value derived from the size distribution. A reasonably good agreement is thus obtained. Moreover, the model, which relates directly the anisotropy of susceptibility to the geometric parameters (d and a) of the system, predicts $\chi_a = 956\,\Phi_0^2$ (to be compared to the fit of the experimental data: $\chi_a = 406\,\Phi_0^2$). Though of the same order of magnitude, the experimental anisotropy appears twice as low as the prediction. This discrepancy could be attributed to the fact that the model assumes a perfectly unidimensional arrangement for the particles: X-ray scattering results [1] show indeed that the particles are depleted from the inner wall of the tubes, but are not perfectly aligned.

5 Determination of elastic constants

We have shown that lyotropic hexagonal phases with magnetic particles trapped inside cylinders display instabilities when submitted to a magnetic field of weak intensity. It is possible through these instabilities to obtain information on the elastic constants of the hexagonal phase. Indeed, the combination of the measurement of the magnetic anisotropy of susceptibility and of the determination of a threshold field (2) enables us to evaluate the product $K_3\left(\bar{B}+C\right)$. One gets: $K_3\left(\bar{B}+C\right) = (6.0\pm3.1)\times10^{-9}\ \mathrm{N^2m^{-2}}$. Moreover, the bending constant K_3 can be estimated through microscopic considerations (though not for doped systems) [5,23]:

$$K_3 \approx \frac{2\pi}{\sqrt{3}}\frac{\kappa R}{d^2},$$

where R is the radius of the cylinders (here $R = 150$ Å), d is the lattice parameter (here $d = 325$ Å) and κ, is the bending rigidity of the surfactant monolayer. Taking for κ the order of magnitude of the thermal energy kT [24], one gets $K_3 = 2\times10^{-13}$ N and thus for the uniaxial compression modulus: $\bar{B}+C = (3.0\pm1.5)\times10^4$ Pa. The elasticity of the doped hexagonal phases is fully discussed elsewhere [25]. Let us simply remark here that this compression modulus appears several orders of magnitude smaller than the compression modulus for a thermotropic hexagonal liquid crystal or for a non-swollen lyotropic hexagonal phase ($\bar{B}+C \sim 10^7$ Pa) [26], but two orders of magnitude larger than the compression modulus for a lamellar phase of very closed composition ($\bar{B}+C \sim 10^2$ Pa) [27].

6 Conclusion

Lyotropic hexagonal phases with magnetic particles inserted inside their cylinders actually achieve unidimensional magnetic fluids. As such, they possess an anisotropy of magnetic susceptibility, whose experimental study is reported here. Both the parallel and perpendicular susceptibilities of the phase are high, as expected from a superparamagnetic medium, and their difference is large as well, showing that the system is indeed strongly anisotropic. The variation of the anisotropy of magnetic susceptibility with the volume fraction of particles can be quantitatively interpreted in the framework of mean-field-type processes, involving the anisotropy of the dipolar magnetic field coupled to the strong anisotropy of spatial distribution for the particles. Because of this high anisotropy of susceptibility, magnetically doped hexagonal samples present very specific features. In particular, instabilities occur for very weak magnetic field, much weaker than for analogous systems such as thermotropic hexagonal phases, whose diamagnetic susceptibilities and relative anisotropy, are several orders of magnitude smaller.

Finally, let us mention that one can take advantage of the rather easy way of orienting hexagonal phases (by annealing under a magnetic field of weak intensity) compared to usual lyotropic phases, to obtain perfectly aligned samples. These latter are suitable for other experiments, as for instance dynamic light scattering [28].

We would like to thank Ian Campbell for the generous disposal of the SQUID magnetometer, Virginie Ponsinet and Madeleine Veyssié for fruitful discussions and Phil N. Segré for a careful reading of the manuscript

References

1. L. Ramos, P. Fabre, R. Ober, Eur. Phys. J. B **1**, 319 (1998).
2. P. Fabre, C. Casagrande, M. Veyssié, V. Cabuil, R. Massart, Phys. Rev. Lett. **64**, 539 (1990).
3. V. Ponsinet, P. Fabre, M. Veyssié, R. Cabanel, J. Phys. II France **4**, 1785 (1994).
4. V. Ponsinet, P. Fabre, M. Veyssié, Europhys. Lett. **30**, 277 (1995).
5. L. Ramos, P. Fabre, Langmuir **13**, 682 (1997).
6. R. Massart, IEEE Trans. Magn. **17**, 1247 (1981).
7. J.C. Bacri, R. Perzynski, D. Salin, V. Cabuil, R. Massart, J. Mag. Mag. Mat. **85**, 27 (1990).
8. R.E. Rosensweig, *Ferrohydrodynamics* (Cambridge University Press, Cambridge, 1985).
9. J.C. Bacri, R. Perzynski, D. Salin, V. Cabuil, R. Massart, J. Mag. Mag. Mat. **62**, 36 (1986).
10. J. Rogers, P.A. Winsor, J. Coll. Int. Sci. **30**, 500 (1969).
11. F. Livoland, Y. Bouligand, J. Phys. France **47**, 1813 (1986).
12. P. Oswald, J.-C. Géminard , L. Lejcek, L. Sallen, J. Phys. France II **6**, 281 (1996).
13. F. Fried, P. Sixou, Mol. Cryst. Liq. Cryst. B **158**, 163 (1988).
14. W. Helfrich, Appl. Phys. Lett. **17**, 531 (1970).
15. J.-P. Hurault, J. Chem. Phys. **59**, 2068 (1973).
16. P.-G. De Gennes, J. Prost, *The Physics of Liquid Crystals*, 2nd ed. (Clarendon Press, Oxford, 1993).
17. M. Kléman, P. Oswald, J. Phys. **43**, 655 (1982).
18. R.M. Bozorth, D.M. Chapin, J. Appl. Phys. **13**, 320 (1942).
19. The calculation is similar to the one developed in the text (see Sect. 4.2) except that the dipolar fields are in that case replaced by the demagnetizing fields, $-D_iM$, $i = (\|, \perp)$ whose origin is the cylindrical shape of the ferrofluid medium. For an infinite cylinder, one has $D_\| = 0$ and $D_\perp = 1/2$, which leads to $\chi_a = 1/2\alpha_0^2\Phi_0^2 = 1/2\chi_\|^2$. The values of χ_a predicted by this model are several times smaller than the experimental ones.
20. M. Widom, H. Zhang, Mat. Res. Soc. Symp. Proc. **248**, 235 (1992).
21. J.D. Jackson, *Classical electrodynamics* (John Wiley & Sons, Inc., New-York, 1962).
22. L. Ramos, Ph.D. Thesis, Université Paris VI, France, 1997.
23. J.V. Selinger, R.F. Bruinsma, Phys. Rev. A **43**, 2910 (1991).
24. J.-M. Di Meglio, M. Dvolaitzky, C. Taupin, J. Phys. Chem. **89**, 871 (1985).
25. L. Ramos, P. Fabre, Progress in Colloid and Interface Science **110**, 240 (1998).
26. L. Sallen, P. Oswald, J.-C. Géminard, J. Malthête, J. Phys. France II **5**, 937 (1995).
27. F. Nallet, D. Roux, C. Quilliet, P. Fabre, S.T. Milner, J. Phys. France II **4**, 1477 (1994).
28. L. Ramos, F. Nallet, C.Y.D. Lu, P. Fabre, in preparation.